Polyhedron 30 (2011) 427–437

Contents lists available at ScienceDirect

Polyhedron

journal homepage: www.elsevier.com/locate/poly

In depth investigation of the synthesis, structural, and spectroscopic characterization of a high pH binary Co(II)–N,N-bis(phosphonomethyl)glycine species. Association with aqueous speciation studies of binary Co(II)–(carboxy)phosphonate systems

M. Menelaou [a], M. Daskalakis [b], A. Mateescu [b], C.P. Raptopoulou [c], A. Terzis [c], C. Mateescu [f], V. Tangoulis [e], T. Jakusch [d], T. Kiss [d,*], A. Salifoglou [a,*]

[a] Laboratory of Inorganic Chemistry, Department of Chemical Engineering, Aristotle University of Thessaloniki, Thessaloniki 54124, Greece
[b] Department of Chemistry, University of Crete, Heraklion 71409, Greece
[c] Institute of Materials Science, NCSR "Demokritos", Aghia Paraskevi, 15310 Attiki, Greece
[d] Biocoordination Chemistry Research Group of the Hungarian Academy of Sciences, Department of Inorganic and Analytical Chemistry, University of Szeged, Szeged H-6720, Hungary
[e] Department of Chemistry, Aristotle University of Thessaloniki, Thessaloniki 54124, Greece
[f] Banat University of Agricultural Sciences and Veterinary Medicine, Timisoara 1900, Romania

ARTICLE INFO

Article history:
Received 3 August 2010
Accepted 4 November 2010
Available online 16 November 2010

Keywords:
Cobalt(II)
(Carboxy)phosphonic acids
Aqueous speciation studies
Magnetic properties
Structure–reactivity

ABSTRACT

Cobalt is an abundant metal ion present in the abiotic and biological world. The chemical reactivity of Co(II) is exemplified through complex interactions with variable molecular mass ligands, including amino acids, peptides, variable nature organic ligands, and/or phospho(nate)-derivatives thereof. Poised to gain insight into the chemical reactivity of Co(II) toward the family of mixed (carboxy)phosphonate-containing ligands, pH-specific aqueous reactions were carried out between Co(II) and N,N-bis(phosphonomethyl)-glycine (NTA2P), leading to a new pH-structural variant species $(NH_4)_3[Co(C_4H_6O_8NP_2)(H_2O)_2]\cdot 4H_2O$ (**1**) at pH 8. Compound **1** was characterized analytically, spectroscopically (FT-IR, UV–Vis, EPR), and magnetically. X-ray crystallography reveals a mononuclear complex of Co(II) in an NO_5 octahedral environment. The solid state magnetic and EPR data on **1** suggest the presence of a high-spin Co(II) in a distorted octahedral geometry, with a ground state of an effective spin $S = 1/2$. The solution UV–Vis and EPR data suggest retention of the integrity of **1**, consistent with the magnetization measurements. Detailed aqueous speciation studies on binary Co(II)–carboxylate (NTA) and all Co(II)–(carboxy)phosphonate (NTA_xP; $x = 1–3$) systems reveal the aqueous distributions of all species involved in the respective systems and project a mononuclear species not unlike that of **1** in the Co(II)–NTA2P system. The structural and chemical attributes of the title complex reflect the (a) pH-dependent chemical reactivity in the binary Co(II)–NTA2P system, and (b) structure–activity correlations in the aqueous media linking both high and low pH-structural variants. To this end, fundamental structural properties influence the reactivity of Co(II) toward phosphonate and mixed carboxyphosphonate ligands and are ultimately exemplified as a function of phosphonate-containing moieties in NTA derivatives. The variably configured species in such binary Co(II)–ligand systems define the pH dependence and nature of interactions between the two reagents, and could serve further as precursors in the design and discovery of new Co(II)–organophosphonate materials of specific structural lattice, spectroscopic, and magnetic properties.

1. Introduction

Over the past years, organophosphonates have emerged as molecules of variable physicochemical properties exemplified in biological and abiotic applications. In the form of aminophosphonates or even carboxyphosphonates they comprise a family of compounds exhibiting a wide array of chemical reactivity, thereby earmarking their potential into the development of materials chemistry and technology. A variety of metal organophosphates have been synthesized, reflecting the versatile coordination properties of these ligands when bound to various metals [1–3]. To this end, broad applications have been pursued through interactions of such types of ligands with metal ions, including ion exchangers, catalysts, small molecular sensors, and non-linear optics [4–8].

Cobalt as a trace element has been encountered as a metal cofactor of the B_{12} coenzyme and vitamin B_{12} molecules [9–12],

* Corresponding authors. Tel.: +30 2310 996 179; fax: +30 2310 996 196 (A. Salifoglou).
E-mail address: salif@auth.gr (A. Salifoglou).

0277-5387/$ - see front matter © 2010 Elsevier Ltd. All rights reserved.
doi:10.1016/j.poly.2010.11.007

and in metalloenzyme systems such as methionine aminopeptidase [13], nitrile hydratases [14], ribonucleotide reductase, and others [15]. In the form of a divalent metal ion, cobalt can interact with variable molecular mass ligands, as a result of which binary and ternary species with diverse structural features arise, contributing to the understanding of the associated chemical reactivity. It is such chemistries that advance the prospect of binary Co(II) complexes serving as synthons for inorganic–organic hybrid materials. In this context, low molecular mass organophosphonate ligands constitute a wide class of molecules the chemical activity of which toward Co(II) deserves due attention owing to (a) the nature of the metal ion itself, and (b) the variable physicochemical attributes of phosphonates. A representative organophosphonate ligand bearing such features is $(H_2O_3P–CH_2)_2N–CH_2–COOH$ (NTA2P). As a carboxy-diphosphonate ligand, N,N-bis(phosphonomethyl) glycine (NTA2P) has already been shown to interact with Co(II) at low to medium pH values [16,17]. The diversity of derived species stands witness to the potential chemical reactivity within the binary Co(II)–NTA2P system and the importance of structural speciation in unraveling new binary and ternary Co(II)–NTA2P pH-specific structural variants. Herein, we report (a) the pH-specific synthesis, spectroscopic, and structural characterization of a new pH-structural variant species $(NH_4)_3[Co(C_4H_6O_8NP_2)(H_2O)_2]\cdot 4H_2O$ (**1**), between Co(II) and the N,N-bis(phosphonomethyl) glycine ligand at high pH values, and (b) aqueous speciation studies on all binary Co(II)–NTA*x*P (*x* = 0–3) systems providing a global picture of the nature and properties of arising complex species including **1**. Both pH-specific synthetic and aqueous solution studies provide an in-depth picture of the requisite binary system, confirm the nature of the anion in **1** and denote the importance of structural speciation approaches poised to (a) delineate interactions between Co(II) and (carboxy)phosphonates, and (b) provide solid state – solution structure correlations for further use in the development of new inorganic–organic materials.

2. Experimental

2.1. Materials and methods

All experiments were carried out in the air. Nano-pure quality water was used for all reactions. $Co(NO_3)_2\cdot 6H_2O$, nitrilotriacetic acid (dubbed NTA), N-(phosphonomethyl) iminodiacetic acid (H_4NTAP dubbed NTAP), N,N-bis(phosphonomethyl) glycine (H_5NTA2P dubbed NTA2P), and nitrilo tris(methylene-phosphonic acid) (H_6NTA3P dubbed NTA3P) were purchased from Aldrich. Ammonia, KOH, and NaOH were supplied by Fluka.

2.2. Physical measurements

FT-infrared spectra were recorded on a Thermo, Nicolet IR 200 FT-infrared spectrometer. UV–Vis measurements were carried out on a Hitachi U2001 spectrophotometer in the range from 190 to 1000 nm. A ThermoFinnigan Flash EA 1112 CHNS elemental analyzer was used for the simultaneous determination of carbon, hydrogen, and nitrogen (%). The EPR spectra of complex **1** in the solid state and in frozen aqueous solutions were recorded on a Bruker ER 200D-SRC X-band spectrometer, equipped with an Oxford ESR 9 cryostat at 9.174 GHz, 10 dB, and in the temperature range from 4 to 70 K. Magnetic susceptibility data were collected on powdered samples of **1** with a Quantum Design SQUID susceptometer in the 1.7–300 K temperature range, under various applied magnetic fields. Magnetization measurements were carried out at three different temperatures in the field range 0–5 T.

2.3. Electrochemical measurements

Cyclic voltammetric measurements were carried out with an Autolab model PGSTAT100 potensiostat–galvanostat. The entire system was under computer control and was supported by the appropriate computer Autolab software GPES, running on Windows. The employed electrochemical cell had platinum (disk) working and auxiliary (wire) electrodes. As reference electrode, a saturated Ag/AgCl electrode was used. The water used in the electrochemical measurements was of nano-pure quality. KNO_3 was used as a supporting electrolyte. Normal concentrations used, were 1–6 mM in electroanalyte and 0.1 M in supporting electrolyte. Purified argon was used to purge the solutions prior to the measurements. Derived E_{pc} and E_{pa} values are reported versus Ag/AgCl electrode.

2.4. Aqueous speciation studies

2.4.1. Potentiometric measurements

Stability constants were determined by pH-metric titration of 25.0 cm^3 samples. The ligand concentrations examined were 0.004 and 0.002 mol dm^{-3}, and the ligand to metal ion molar ratios were 4:1, 2:1, and 1:1. Titrations were performed over the pH range 1.5–12.0 with a carbonate-free KOH solution (normal titration) or with an HCl solution (back titration) of known concentration (*ca.* 0.2 mol dm^{-3}) under a purified argon atmosphere. In order to check that no oxidation of Co(II) to Co(III) by dioxygen occurs, the reversibility of the titrations in some cases was checked by back titration of the basic solution with strong acid. These titration curves were also included in the calculation of the stability constants. Duplicate titrations were carried out to check the reproducibility of the pH-metric measurements. The reproducibility of titration points included in the evaluation was within 0.005 pH units in the entire pH range. For the potentiometric titration, an automatic titration set including a Dosimat 665 (Metrohm) autoburette, an Orion 710A precision digital pH-meter and an IBM compatible personal computer were used. An Orion 9103BN or a Metrohm 6.0234.100 type semimicro combined pH electrode was calibrated for the hydrogen ion concentration according to the method of Irving et al. [18]. The difference between pH meter readings and $\log[H^+]$ was constant in the pH range 2–4 and 10–11.6. Thus, the junction potential proved to be constant, albeit not negligible, as discussed previously [19]. Concentration stability constants $\beta_{pqr} = [M_pL_qH_r]/[M]^p[L]^q[H]^r$ were calculated through the aid of the PSEQUAD computer program [20,21].

2.4.2. Spectroscopic measurements

Since the interactions of Co(II) with the ligands studied are not so strong as with the previously studied Cu(II), VO(IV), and Al(III) ions, and the potential danger of oxidation of the metal ion increased the uncertainty of the potentiometric titrations, complex formation was concurrently monitored spectrophotometrically by measuring the UV–Vis absorption of the same samples studied pH-metrically in the wavelength range 300–800 nm. A special titration cell was constructed for these measurements consisting of a light tube, with quartz windows on both ends (path length = 3.005 cm), built into a conventional water-jacketed potentiometric cell. In this way, pH-metric and spectrophotometric titrations could be carried out in the same sample. The titration system was kept under an argon atmosphere in order to avoid oxidation of Co(II) to Co(III). This could be easily checked by UV–Vis spectroscopy due to the lack of the intense absorption in the wavelength range <400 nm, characteristic for octahedral Co(III) complexes. The spectral data were evaluated with the PSEQUAD computer program [20,21] to obtain the stability constants (and also the individual spectrum) of complexes formed in the investigated metal–ligand systems. Finally, a joint evaluation of the pH-metric and

spectrophotometric data took place and each data set was accepted as the best one describing the speciation for a specific binary system.

The UV–Vis spectrophotometric data could be used to obtain information about (a) the geometry of the complexes formed between Co(II) and nitrilotriacetic acid, N-(phosphonomethyl) iminodiacetic acid, N,N-bis(phosphonomethyl) glycine, and nitrilo tris(methylene-phosphonic acid) derivatives, and (b) the changes in the binding mode of the complexes formed. Electronic absorption spectra of the complexes formed in the Co(II)–ligand systems were recorded on a Hewlett–Packard 8452 diode-array spectrometer.

2.5. Synthesis of complex $(NH_4)_3[Co(C_4H_6O_8NP_2)(H_2O)_2]\cdot 4H_2O$ (**1**)

A sample of 0.17 g (0.58 mmol) of $Co(NO_3)_2\cdot 6H_2O$ and 0.16 g (0.59 mmol) of N,N-bis(phosphonomethyl) glycine (NTA2P) were dissolved in 5 ml of nano-pure water. The pH of the resulting solution was adjusted to 8 using aqueous ammonia. The reaction mixture was stirred at room temperature for about 30 min. Subsequently, the reaction flask was placed at 4 °C in the presence of ethanol. As a result, several weeks later pink crystals were deposited. The crystalline material was collected by filtration and dried under vacuum. Yield: 0.16 g (~59%). *Anal.* Calc. for $(NH_4)_3[Co(C_4H_6O_8NP_2)(H_2O)_2]\cdot 4H_2O$ (**1**) ($C_4H_{30}CoN_4O_{14}P_2$, MW = 479.19): C, 10.03; H, 6.31; N, 11.69. Found: C, 10.04; H, 6.33; N, 11.64%.

2.6. X-ray crystallography

2.6.1. Crystal structure determination

X-ray quality crystals of compound **1** were grown from water–ethanol solutions. A single crystal, with dimensions 0.04 × 0.18 × 0.28 mm was mounted on a Crystal Logic dual-goniometer diffractometer, using graphite monochromated Mo Kα radiation. Unit cell dimensions for **1**, were determined and refined by using the angular settings of 25 automatically centered reflections in the range $11 < 2\theta < 23°$. Crystallographic details are given in Table 1. Intensity data were measured by using $\theta - 2\theta$ scans. Throughout data collection, three standard reflections were monitored every 97 reflections, and showed less than 3% variation and no decay. Lorentz, polarization corrections were applied by using CRYSTAL LOGIC software. Further experimental crystallographic details for **1**: $2\theta_{max} = 46°$; number of reflections collected/unique/used, 2641/2536[R_{int} = 0.0636]/2536; 299 parameters refined; $F(0\,0\,0)$ = 1004; $(\Delta/\sigma)_{max}$ = 0.009; $(\Delta\rho)_{max}/(\Delta\rho)_{min}$ = 0.692/−1.229 e/Å^3; GOF = 1.098; R/R_w (for all data), 0.0919/0.2171.

The structure of complex **1** was solved by direct methods using SHELXS-97 [22], and refined by full-matrix least-squares techniques on F^2 with SHELXL-97 [23]. All non-H atoms in the structure of **1** were refined anisotropically. All H-atoms in the structure of **1** were located by difference maps and were refined isotropically.

Table 1
Summary of crystal, intensity collection and refinement data for $(NH_4)_3[Co(C_4H_6O_8NP_2)(H_2O)_2]\cdot 4H_2O$ (**1**).

Formula	$C_4H_{30}CoN_4O_{14}P_2$
Formula weight	479.19
T (K)	298
Wavelength	Mo Kα 0.71073
Space group	$P2_1/n$
a (Å)	11.633(7)
b (Å)	10.670(6)
c (Å)	15.87(1)
α (°)	90.0
β (°)	109.24(2)
γ (°)	90.0
V (Å^3)	1860(2)
Z	4
D_{calc} (mg m^{-3})	1.712
Absorption coefficient (μ) (mm^{-1})	1.168
Range of h,k,l	−12 → 12, −11 → 0, 0 → 17
R[a]	R = 0.0755[b]
R_w[a]	R_w = 0.1950[b]

[a] R values are based on F values, R_w values are based on F^2. $R = \frac{\sum||F_o|-|F_c||}{\sum(|F_o|)}$, $R_w = \sqrt{\frac{\sum[w(F_o^2-F_c^2)^2]}{\sum[w(F_o^2)^2]}}$.

[b] [2017 Refs. $I > 2\sigma(I)$].

3. Results

3.1. Synthesis

Complex **1** has been synthesized *via* a facile pH-specific reaction between Co(II) and N,N-bis(phosphonomethyl) glycine with a 1:1 M ratio. The overall reaction leading to the isolation of **1** is shown below:

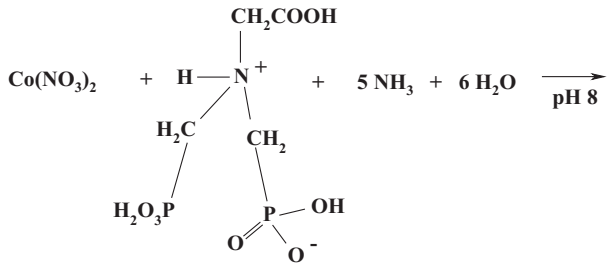

$$(NH_4)_3[Co(C_4H_6O_8NP_2)(H_2O)_2]\cdot 4\,H_2O \quad + \quad 2\,NH_4NO_3$$

Elemental analysis on the pink-colored crystalline product suggested the formulation $(NH_4)_3[Co(C_4H_6O_8NP_2)(H_2O)_2]\cdot 4H_2O$ (**1**). Ammonia was crucial in the investigated reaction. It not only helped to adjust the pH of the reaction mixture, but it also provided the necessary counterions to balance the arisen negative charge of the anionic complex. All of these points were subsequently proven by X-ray crystallography. The crystals isolated from the reaction mixture are stable in the air for long periods of time, with no visible deterioration. The title complex is soluble in water and insoluble in alcohols (CH_3OH, *i*-PrOH, etc.), acetonitrile, and dimethyl sulfoxide (DMSO).

3.2. Description of crystal structure of $(NH_4)_3[Co(C_4H_6O_8NP_2)(H_2O)_2]\cdot 4H_2O$ (**1**)

The X-ray crystal structure of **1** reveals the presence of discrete anions $[Co(C_4H_6O_8NP_2)(H_2O)_2]^{3-}$ and NH_4^+ counterions. The DIAMOND diagram of **1** is shown in Fig. 1. Selected interatomic distances and angles for **1** are listed in Table 2. The structure consists of a mononuclear complex of Co(II). The coordination sphere of the central metal ion Co(II) is formulated by the organophosphonate ligand N,N-bis(phosphonomethyl) glycinate ($^{=}O_3P–CH_2–N(CH_2COO^-)–CH_2–PO_3^{=}$ = NTA2P^{5-}). Thus, one NTA2P^{5-} ligand employs the two phosphonate groups to coordinate to Co(II) through both of its doubly deprotonated hydroxides, the imino nitrogen atom and the remaining carboxylate group participating in monodentate coordination. Since both phosphonate groups are doubly deprotonated, three ammonium ions counteract the generated 3− charge of the arising anionic complex. Two water molecules complete the distorted octahedral coordination geometry around the Co(II) ion.

The Co–O distances in **1** are similar to those observed in other octahedral Co(II) sites, among which are those in $[Co(C_2H_8O_6NP_2)_2(H_2O)_2]$ (2.067(2)–2.132(2) Å) (**2**) [24], $[Co(C_4H_9O_8NP_2)$

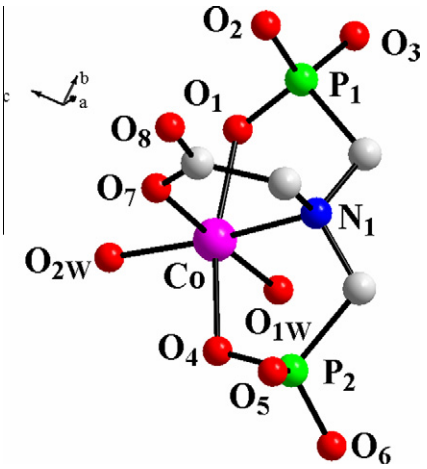

Fig. 1. Crystal structure of the anion in $(NH_4)_3[Co(C_4H_6O_8NP_2)(H_2O)_2]\cdot 4H_2O$ (**1**). Thermal ellipsoids are drawn by DIAMOND and represent 50% probability surfaces.

Table 2
Selected bond lengths (Å) and angles (°) in $(NH_4)_3[Co(C_4H_6O_8NP_2)(H_2O)_2]\cdot 4H_2O$ (**1**).

Bond distances (Å)			
Co–O(1)	2.129(6)	Co–N(1)	2.181(6)
Co–O(4)	2.103(5)	Co–O(1w)	2.056(7)
Co–O(7)	2.041(6)	Co–O(2w)	2.095(5)
Angles (°)			
O(7)–Co–O(4)	93.3(2)	O(1w)–Co–O(2w)	90.8(2)
O(7)–Co–O(1)	92.6(2)	O(1w)–Co–O(4)	87.2(2)
O(4)–Co–O(1)	168.4(2)	O(2w)–Co–O(4)	96.5(2)
O(7)–Co–N(1)	81.5(2)	O(1w)–Co–O(1)	86.5(2)
O(4)–Co–N(1)	84.9(2)	O(2w)–Co–O(1)	93.4(2)
O(1)–Co–N(1)	86.1(2)	O(1w)–Co–N(1)	96.2(2)
O(7)–Co–O(1w)	177.6(2)	O(2w)–Co–N(1)	172.9(3)
O(7)–Co–O(2w)	91.5(2)		

$(H_2O)_2]\cdot 2H_2O$ (2.100(2)–2.141(2) Å) (**3**) [16], $(NH_4)_4[Co(H_2O)_6][(H_2O)_2Co(HNTA2P)Co(NH_3)_2(H_2O)_3]_2[Co(NTA2P)(H_2O)_2]_2\cdot 10H_2O\cdot 1.36CH_3CH_2OH$ (2.060(3)–2.147(3) and 2.073(4)–2.117(3) Å) (**4**) [17], $(NH_4)_4[Co(C_6H_5O_7)_2]$ (2.051(2)–2.157(2) Å) (**5**) [25], $[Co\{COOCH_2CH(OH)COO\}]\cdot 3H_2O$ (2.067(3)–2.136(3) Å) (**6**) [26], and the phosphonate derivatives $[Co(NH_3CH_2PO_3)_2(H_2O)_2]$ (2.104(4)–2.121(4) Å) (**7**) [27], $[Co(HO_3PC(CH_3)(OH)PO_3H)_2\text{-}(H_2O)_2]$ $[NH_2(C_2H_5)_3]_2$ (2.064(2)–2.179(2) Å) (**8**) [28]. Moreover, the M(II)–O distances are similar to those in other complexes including $\{NH_3CH_2CH_2NH_3\}\cdot\{Ni[O_2CCH_2N(CH_2PO_3H)_2](H_2O)_2\}_2$ (2.028(6)–2.097(6) Å) (**9**) [29].

The angles within the equatorial plane in **1** are in the range 84.9(2)–96.5(2)°, and hence stand variably spread around the ideal octahedral angle of 90°. The aforementioned angle values are similar to those observed in (**2**)–(**8**) and the heterometal complexes $[Cu(HO_3PC(CH_3)(OH)PO_3H)_2]^{2-}$ (84.7–95.3° and 87.8–92.2°, respectively) [30] and $[Zn(HO_3PC(CH_3)(OH)PO_3H)_2]^{2-}$ (85.0–95.0° and 88.6–91.4°, respectively) [30].

Hydrogen bonding interactions are present in the crystal structure of **1** (Table 3). These interactions involve the coordinated water molecules, the ammonium counterions, and the phosphonate and carboxylate oxygen atoms of the NTA2P^{5-} ligand. Collectively, the hydrogen bonds generate an extensive network, which likely contributes to the overall stability of the crystal lattice (Fig. 2) in **1**.

3.3. Electronic spectroscopy

The UV–Vis spectrum of **1** was recorded in water (see Supporting Information). The spectrum exhibits a major peak at λ_{max} = 540 nm, a well-discernible shoulder around 478 nm, and a strongly absorbing band rising into the UV with a maximum at 220 nm. The absorption features in the low energy region are likely due to d–d transitions, which are typical for a Co(II) d^7 octahedral species [31]. The absorption features around 500 nm could be tentatively attributed to the $^4T_{1g} \rightarrow {}^4T_{1g}(P)$ transition. The observed multiple structure is in line with literature reports invoking (a) admixture of spin forbidden transitions to doublet states derived from ^2G and ^2H, (b) spin–orbit coupling, and (c) vibrational or low symmetry components, to account for the complexity of the spectrum [32]. In the absence of detailed studies no further assignments could be proposed. The spectrum of **1** in water is different from that of $Co(II)_{aq}$ [33] reflecting the unique coordination sphere composition of Co(II) in solution.

3.4. FT-IR spectroscopy

The FT-infrared spectrum of complex **1**, in KBr, shows strong absorptions for the various vibrationally active groups. Antisymmetric as well as symmetric vibrations for the carboxylate group of the coordinated NTA2P^{5-} ligand dominated the spectrum. Specifically, antisymmetric stretching vibrations $\nu_{as}(COO^-)$ were present for the carboxylate carbonyls around 1590 cm^{-1}. Symmetric vibrations $\nu_s(COO^-)$ for the same group were present in the range 1400–1381 cm^{-1}. The frequencies of the observed carbonyl vibrations were shifted to lower values in comparison to the corresponding vibrations in the free NTA2P acid. The difference between the symmetric and antisymmetric stretches, $\Delta(\nu_{as}(COO^-)$–$\nu_s(COO^-))$, was greater than 200 cm^{-1}, indicating that the carboxylate group of the NTA2P^{5-} ligand was either free or coordinated to the metal ion in a monodentate fashion [34]. This contention was further confirmed by the X-ray crystal structure of **1**. Vibrations for the PO_3 groups are observed for the antisymmetric stretching vibrations $\nu_{as}(PO_3)$ between 1088 and 1053 cm^{-1}. Symmetric stretching vibrations $\nu_s(PO_3)$ are observed in the range 974–915 cm^{-1}. The frequencies for the aforementioned stretches appear to be shifted to lower values compared to those of free NTA2P acid, indicating changes in the vibrational status of the ligand upon coordination to the Co(II) ion [35,36]. The aforementioned tentative assignments are, also, in consonance with previous results reported for iminophosphonate containing complexes of Co(II) and various metals [37].

3.5. Magnetic susceptibility studies

3.5.1. Magnetic susceptibility

Fig. 3 shows the $\chi_M T$ versus T susceptibility data at 0.7 T, while the solid line represents the fit according to the following general Hamiltonian (Eq. (1)):

$$H = D\left[S_z^2 - \frac{1}{3}S(S+1)\right] + E(S_x^2 - S_y^2) + g\mu_B H\cdot S \qquad (1)$$

where all the parameters have their usual definitions, and $S = 3/2$.

The $\chi_M T$ values decrease smoothly from 3.07 emu mol^{-1} K at 300 K to 2.70 emu mol^{-1} K at 98 K and then more steeply to the value of 1.6 emu mol^{-1} K at 2.0 K. The high-temperature value of $\chi_M T$ is higher than 1.875 emu mol^{-1} K, the value that would be expected for a Co(II) system with an $S = 3/2$. This behavior is consistent with the presence of a significant orbital contribution to the anisotropic nature of the investigated Co(II) system. The employed fitting model for the susceptibility data is shown in [Eq. (1)]. The model takes into account (a) both the axial and rhombic parts of distortion of the crystal field (D, E), and (b) an isotropic g-value, with the fitting results yielding the following parameters: $D = 70(1)$ cm^{-1} and $g = 2.5(1)$. The theoretical curve is shown as a

Table 3
Hydrogen bonds in **1**.

Interaction	H···A (Å)	D···A (Å)	D–H···A (°)	Symmetry operation
O1w–H1wA···O3w	1.919	2.657	156.8	$x, 1+y, z$
O1w–H1wB···O4	1.839	2.692	176.1	$1-x, -y, 1-z$
O2w–H2wA···O2	1.872	2.682	174.1	$1.5-x, -0.5+y, 1.5-z$
O2w–H2wB···O6	1.991	2.795	167.4	$1-x, -y, 1-z$
O3w–H3wA···O3	1.748	2.716	161.2	$1-x, -y, 1-z$
O3w–H3wB···O8	1.947	2.752	151.8	$-0.5+x, -0.5-y, -0.5+z$
O4w–H4wA···O5	1.927	2.744	171.3	x, y, z
O4w–H4wB···O6w	2.158	2.781	132.2	$0.5+x, -0.5-y, 0.5+z$
O5w–H5wA···O5	2.014	2.696	170.5	x, y, z
O5w–H5wB···O3	1.893	2.794	176.3	$x, -1+y, z$
O6w–H6wA···O8	1.930	2.700	178.1	$2-x, -y, 1-z$
O6w–H6wB···O6	1.887	2.700	154.0	x, y, z
N2–H2wA···O1	2.220	2.879	140.7	$1.5-x, -0.5+y, 1.5-z$
N2–H2wB···O3	2.117	3.028	155.8	$x, -1+y, z$
N2–H2wC···O4	1.703	2.816	174.0	x, y, z
N2–H2wD···O4w	2.098	2.902	157.5	x, y, z
N3–H3wA···O6	2.035	2.891	175.0	x, y, z
N3–H3wB···O1	1.769	2.805	167.9	$1-x, -y, 1-z$
N3–H3wC···O3	2.037	3.107	168.9	$x, -1+y, z$
N3–H3wD···O8	2.540	3.233	155.1	$-0.5+x, -0.5-y, -0.5+z$
N4–H4wA···O6w	2.208	3.047	154.7	x, y, z
N4–H4wB···O5w	1.859	2.746	169.4	$1.5-x, 0.5+y, 0.5-z$
N4–H4wC···O2	1.803	2.703	178.0	$-0.5+x, 0.5-y, -0.5+z$
N4–H4wD···O6w	2.458	3.237	144.7	$1.5-x, 0.5+y, 0.5-z$

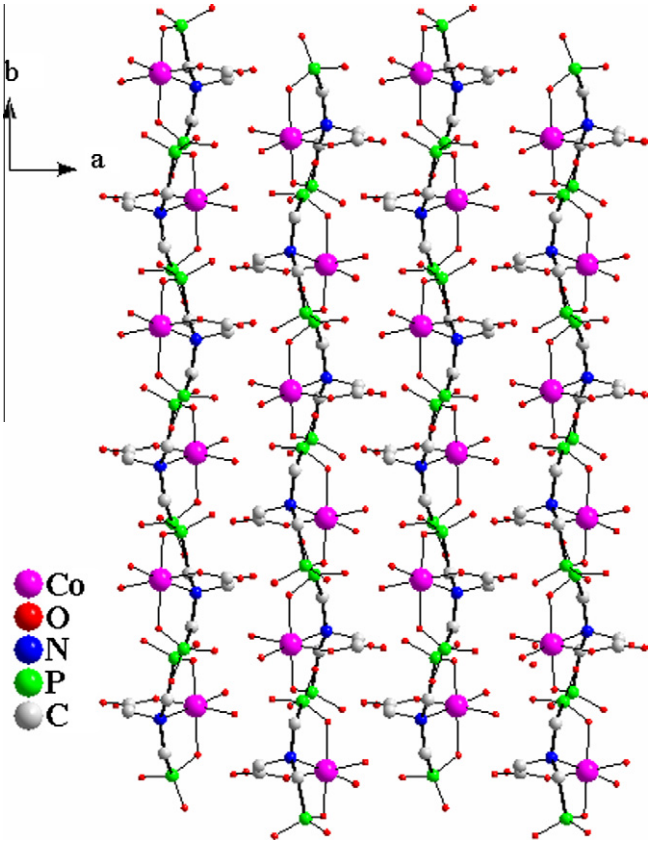

Fig. 2. Development of parallel chains of the anion of **1** in the *ab* plane of the crystal lattice.

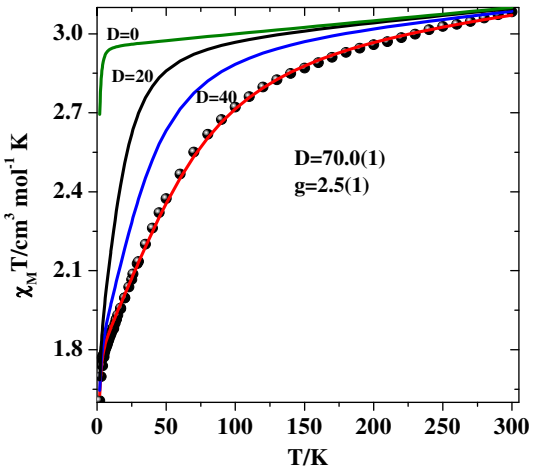

Fig. 3. Temperature dependence of the magnetic susceptibility of **1**, in the form of $\chi_M T$ versus T, in the temperature range 1.7–300 K using an external magnetic field of 0.7 T. The solid line represents the fitting results. Different simulations of the susceptibility equation for different values of the D parameter (D = 0, 20, 40) are also shown as solid lines (see text).

solid line in the same figure. Therein, various simulations with different values of the D parameter (and the same g-value) are also shown. It must be pointed out that the sign of the D parameter along with the E parameter are not resolved from the magnetic measurements, while introduction of an axial symmetry to the g-parameter ($g_\perp$, $g_{||}$) leads to no improvement of the fit. The large value of the D parameter is in accordance with an octahedral Co(II), where the ground state doublet is well-isolated from the excited ones [38].

3.6. Magnetization studies

The magnetization data for **1** in the form of $M/N\mu_B$ versus H/T, are shown in Fig. 4, at 2 K and in the field range 0–5 T. The dotted line represents the theoretical magnetization curves for a system having a ground state with an effective spin $S = 1/2$ and effective g value equal to 4.33. The ground state of the free high-spin Co(II) ion in an octahedral environment is ^{4}F, but the orbital degeneracy is removed in an octahedral crystal field yielding one ^{4}A and two ^{4}T levels, with the lowest-lying state being a $^4T_{1g}$. The degeneracy of the $^4T_{1g}$ level is removed through the action of axial and rhombic distortions of the crystal field as well as through spin–orbit

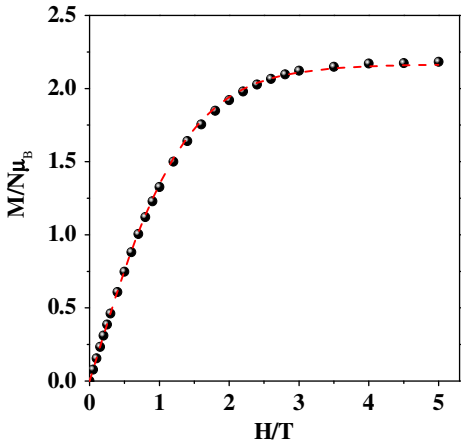

Fig. 4. Magnetization of **1**, in the form of $M/N\mu_B$ versus H/T, at 2 K and in the field range 0–5 T. The solid line represents the theoretical Brillouin functions for an isolated $S = 1/2$ system with a g_{eff} 4.33.

coupling. The overall effect of low symmetry crystal-field components and spin–orbit coupling produces six Kramers doublets and results in a doublet ground state. Since (a) the same doublet energy level remains lowest in energy for all values of the applied field strength, and (b) the energy difference between the two lowest lying doublets is relatively large with respect to the thermal energy present at low temperatures (<30 K), the Co(II) system may be described as one having a ground state with an effective spin of $S = 1/2$. Since there is no discrepancy between the theoretical and the experimental curves, intermolecular interactions are of no-importance in the low temperature regime.

3.7. EPR spectroscopy

X-band EPR measurements were carried out in powder samples as well as in frozen solutions of **1** in water and are shown in Figs. 5 and 6, respectively. As a consequence of the fast spin–lattice relaxation time of high-spin Co(II), signals were observed only below 70 K. For the powder spectra, at temperatures $T < 25$ K, a rather complicated spectrum appears with many signals at low fields, making it quite difficult to follow the usual simulation procedure [39].

The dominant broadening effect emerges when the g-strain is converted into B-strain through the equation $\Delta B = -(\frac{h\nu}{\mu_B})(\frac{\Delta g}{g^2})$, where the parameters have their usual meaning. Thus, the largest and smallest g-values of the powder and solution spectra have field widths that differ by an order of magnitude, thereby rationalizing the broad high-field features of the spectrum. It is clear that the system retains its structure in solution, with the g strain effect being the dominant factor responsible for the observed shift of the g value of the derivative signal (4.3(1) in the solid state and 3.7(1) in solution) upon passing from the solid to the solution state.

A very important feature of the Co(II) ion is the value of the effective *g-parameter*, g_{eff}, extracted from the EPR measurements, as a result of which interesting comments can be made about the influence or not of intermolecular interactions on that parameter [16]. It was shown that for values of $g_{eff} > 4.3(1)$ (in the EPR spectra of Co(II) complex powder samples), the intermolecular interactions contribute significantly to the magnetic behavior of the system, while for all the other cases ($g_{eff} < 4.3(1)$) no significant intermolecular interactions are observed. Although it was not possible to derive a g_{eff} value from the powder EPR spectrum, the simulation of the magnetization curve gave a value of g_{eff} close to 4.3(1), which shows that intermolecular interactions are not significant (a Brillouin function of an isolated $S = 1/2$ system could reproduce the magnetization).

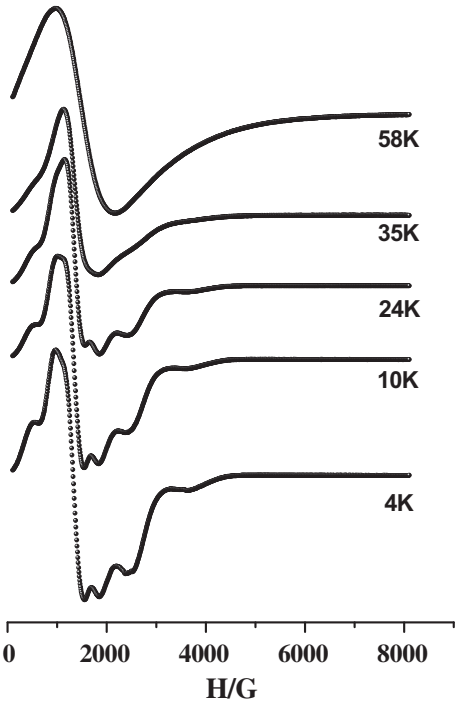

Fig. 5. Temperature dependence of the powder X-band EPR spectrum of **1** in the field range 0–8000 Oe.

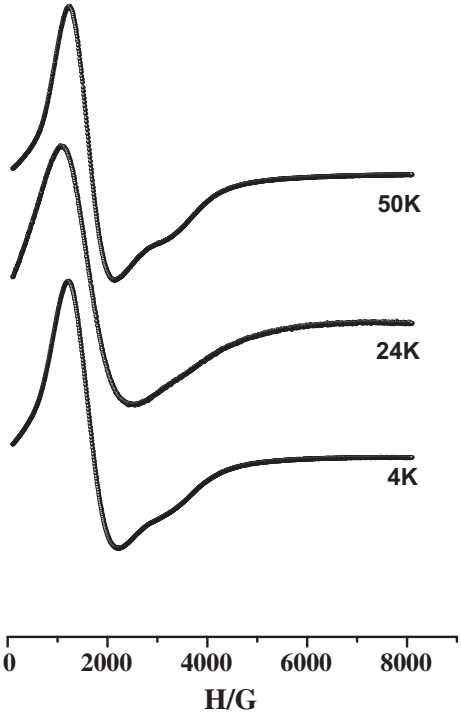

Fig. 6. Temperature dependence of the frozen water solution X-band EPR spectrum of **1** in the field range 0–8000 Oe.

Another important aspect of this study [16] is the derivation of the D parameters for various Co(II) complexes. In the specific case of the low pH-structural variant $[Co(C_4H_9O_8NP_2)(H_2O)_2]\cdot 2H_2O$ (**3**) [16] it was shown that the D value is 41 cm^{-1}, while

in the case of **1** the D value is higher (*ca.* 70 cm^{-1}). This difference could be easily explained by the larger crystal field effect expected in **1** due to the deprotonated character of the ligand in the complex.

3.8. Cyclic voltammetry

The cyclic voltammetry of complex **1** was studied in aqueous solutions, in the presence of KNO_3 as a supporting electrolyte. The cyclic voltammogram of **1** (scan rate 200 mV/s) exhibits an ill-defined electrochemical behavior with an irreversible wave at −0.64 V versus Ag/AgCl. The observed irreversibility reflects complex electrochemical processes, involving Co(II)/Co(I) redox state and coordination number changes. Attempts to pursue the isolation of reduced products of **1** are currently ongoing.

3.9. Aqueous speciation

3.9.1. Protonation equilibria

A maximum of four protons in the NTA and a commensurate number of protons in its phosphonate derivatives are involved in deprotonation processes in the measurable pH range (see Table 4). The proton dissociation constants of the studied ligands (listed in Table 4) are the mean values of the data determined by us in the past [40–42] as well as in the herein reported work. The data are in good agreement with those reported previously and they are within the indicated experimental error [41–43]. The pK values of the PO_3H_2 groups are ∼1 or lower and have not been determined in these cases. One of the carboxylic functions of each ligand (except NTA3P) is deprotonated in the pH range 2–3.5; the acidity of these groups increases along with the number of phosphonate groups. The pK values of the second (NTA, NTAP) and the third (NTA) carboxylic functions are lower than 2 and these values, if at all, can be determined pH-metrically only with rather high uncertainties. Moreover, the ensuing deprotonations occur in the pH range 4–7 and correspond to the PO_3H^- groups. Therefore, the most basic donor is the tertiary amino group in the aforementioned ligands with pK values 9.5–12.3 (see Table 4). In addition, basicity increases with increasing number of phosphonate groups, due to their negative charge and electron repelling effect [41–43].

Table 4
Proton dissociation constants and Co(II) complex formation constants of NTA and its phosphonic acid derivatives at 25 °C and I = 0.20 mol dm^{-3} (KCl). The pK values of the studied ligands are the average of the data determined by us in the past as well as in the herein reported work.

	NTA	NTAP	NTA2P	NTA3P
pK_{NH^+}	9.58(7)	10.53(1)	11.54(12)	12.3[a]
$pK_{PO_3H^-}$	–	5.48(3)	6.30(6)	7.03(11)
$pK_{PO_3H^-}$	–	–	4.90(5)	5.70(3)
$pK_{PO_3H^-}$	–	–	–	4.47(5)
pK_{COOH}	2.43(7)	2.29(3)	1.95(14)	–
pK_{COOH}	1.78(10)	1.32(10)	–	–
pK_{COOH}	1.2(2)	–	–	–
$CoAH_3$	–	–	–	27.94(8)
$CoAH_2$	–	–	22.42(7)	24.38(6)
CoAH	–	16.11(6)	17.97(5)	19.49(4)
CoA	9.80(6)	11.04(5)	12.55(4)	13.67(5)
$CoAH_{-1}$	−1.41(5)	−0.45(6)	0.25(5)	
CoA_2	13.76(7)	13.54(9)	–	–
pK_{CoAH_3}	–	–	–	3.55
pK_{CoAH_2}	–	–	4.45	4.90
pK_{CoAH}	–	5.07	5.42	5.81
pK_{CoA}	11.22	11.49	12.30	>13[b]

[a] Taken only from the references, this value could not be fit in this particular case.
[b] Estimated value.

3.9.2. Co(II)–NTA_xP complex formation processes

The species distribution curves for the complexes formed in the binary systems of Co(II)–(NTA-type) and aminophosphonate derivative ligands, are depicted in Figs. 7–10, and the stability constants as well as the spectral parameters can be found in Tables 4 and 5, respectively. The NTA-like ligands are potentially tetradentate metal ion binders [41–43], and do not prefer to form bis-complexes in comparison with the corresponding iminodiacetic derivatives [41–43]. Bis-complex formation grows less and less likely as the number of phosphonate groups increases. CoA_2 bis-complex formation can be observed only in the case of the Co(II)–NTA and Co(II)–NTAP systems. Coordination of the second ligand is hindered, however, as that is demonstrated by the very low log K(CoA_2) values 3.96 and 2.50, and very large log [K(CoA)/K(CoA_2)] values = 5.84 and 8.53, respectively. The spectral parameters of the CoA_2 bis-complexes resemble those projecting a usual octahedral geometry (Table 5B).

Furthermore, as more COO^- groups are replaced by PO_3^{2-} groups, there is a higher tendency for the ligands to form protonated complexes. While for NTA, no protonated complex can be observed, in the case of mixed carboxyphosphonate derivatives (NTAP and NTA2P) the CoAH (and the $CoAH_2$) species appears in a high amount (at least ∼60%). In the case of the binary Co(II)–NTA3P system, the $CoAH_3$ species forms at a significant concentration at pH 3.5–4. The relatively low values of the stepwise protonation constants in the series CoA → CoAH → $CoAH_2$ → $CoAH_3$ suggest that protonation occurs at the phosphonate arms, while the nitrogen atom remains coordinated. The same behavior had been previously observed in the case of the corresponding Cu(II) complexes [40]. However, the coordination of all phosphonate groups of the NTA3P ligands to Co(II) ions is not likely.

The first complex formed in the binary Co(II)–NTAxP (x = 0, NTA; x = 1, NTAP; x = 2, NTA2P) system has very similar spectral parameters in all cases (λ_{max} 514–516 nm, ε 16–22 mol^{-1} dm^3 cm^{-1}) (Table 5A). This species, presumably as in the case of NTA, reveals a (N, $(COO^-)_{3-x}$) binding mode with all ligand molecules, however the partial coordination of the protonated phosphonate residue can not be excluded. In the first deprotonation process (x = 1,2), one phosphonate enters the coordination sphere of the metal ion and the spectrum changes, exhibiting a feature at λ_{max} = 538 nm, ε = 30–38 mol^{-1} dm^3 cm^{-1}. The deprotonation and probably coordination of the second phosphonate group in the case of NTA2P causes a further increase (ε 20.6 mol^{-1} dm^3 cm^{-1}) in the molar absorbance, while λ_{max} hardly changes (∼2 nm). The spectral parameters of the Co(II)-complexes with NTA3P do not follow this "trend": the molar absorbance of the first species ($CoAH_3$) is much higher than the others. The deprotonations in the other cases cause

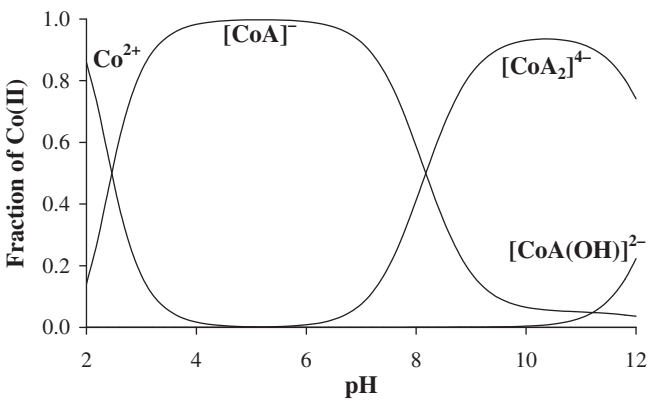

Fig. 7. Speciation curves for complexes forming in the Co(II)–NTA system; c_{Co} = 0.001 mol dm^{-3}, c_{ligand} = 0.004 mol dm^{-3}. Charges are omitted for clarity.

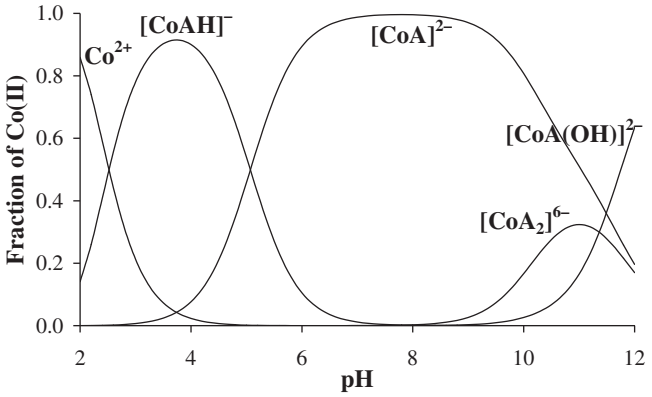

Fig. 8. Speciation curves for complexes forming in the Co(II)–NTAP system; c_{Co} = 0.001 mol dm^{-3}, c_{ligand} = 0.004 mol dm^{-3}. Charges are omitted for clarity.

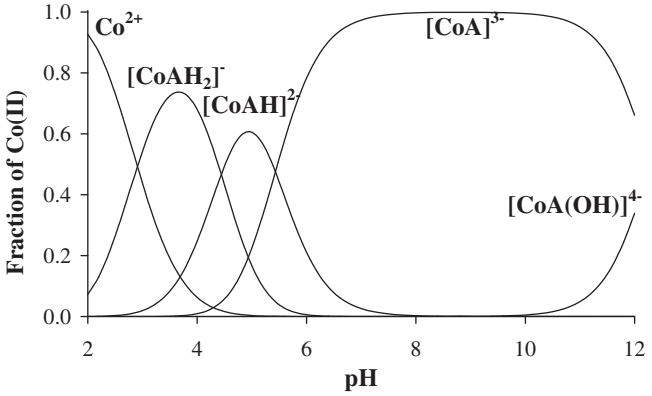

Fig. 9. Speciation curves for complexes forming in the Co(II)–NTA2P system; c_{Co} = 0.001 mol dm^{-3}, c_{ligand} = 0.004 mol dm^{-3}. Charges are omitted for clarity.

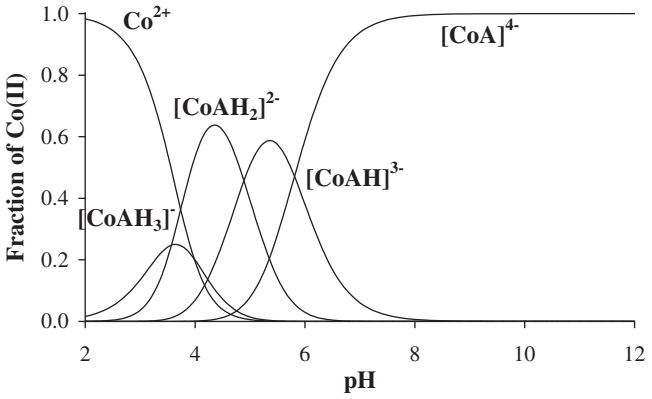

Fig. 10. Speciation curves for complexes forming in the Co(II)–NTA3P system; c_{Co} = 0.001 mol dm^{-3}, c_{ligand} = 0.004 mol dm^{-3}. Charges are omitted for clarity.

increase of the molar absorbance (16–21 mol^{-1} dm^3 cm^{-1}). In this case, the molar absorbance decreases first, then it increases a little (8 mol^{-1} dm^3 cm^{-1}) and finally it decreases again.

As the pH increases, the species CoA undergoes further deprotonation to form complexes $CoAH_{-1}$ (x = 1–3), and a significant color change from pink to bluish green (reflected in the spectral parameters shown in Table 5B) indicates formation of mixed hydroxo complexes (see Figs. 2–4 Supporting Information); based on the spectral parameters the geometry of these species is tetrahedral.

Table 5
The UV–Vis spectroscopic data on the individual complexes formed in the Co(II)–NTA and phosphonate derivative systems at 25 °C and I = 0.20 mol dm^{-3} (KCl).

Ligand	λ_{max}				ε_{max}			
	CoA	CoAH	$CoAH_2$	$CoAH_3$	CoA	CoAH	$CoAH_2$	$CoAH_3$
NTA	514	–	–	–	22.0	–	–	–
NTAP	538	514	–	–	37.5	18.3	–	–
NTA2P	540	538	516	–	52.7	32.1	16.1	–
NTA3P	536	538	538	542	37.0	38.4	29.9	42.9

Ligand	$CoAH_{-1}$					CoA_2	
	λ_{max1}	ε_{max1}	λ_{max2}	ε_{max2}	$\varepsilon_{max2}/\varepsilon_{max1}$	λ_{max}	ε_{max}
NTA	632	65.8	496	47.7	0.73	514	12.2
NTAP	628	83.1	508	67.3	0.81	518	12.9
NTA2P	618	64.3	518	63.3	0.98	–	–
NTA3P[a]	~600	59.5	532	43.3	~1.4	–	–

[a] The species $CoAH_{-1}$ probably forms with NTA3P too. However, the observed ~5% formation at pH ~12.0 is not enough to determine accurate spectral parameters.

4. Discussion

4.1. Synthetic and structural chemistry in the Co(II)–NTA2P binary system

The interaction between metal ions, such as Co(II), and various phosphonate ligands has been a challenge in research over the past few years. In the case of the family of phosphonates originating in the tricarboxylic acid NTA, a specific derivative, i.e. NTA2P, has been the focus of investigation in the presence of Co(II) ions. Given the fact that NTA2P possesses five protons capable of undergoing deprotonation as a function of pH and could coordinate metal ions through various binding modes, the chemical reactivity of the binary Co(II)–NTA2P system was probed through a thorough structural speciation approach. In this regard, synthetic efforts in this system were launched as a function of pH in aqueous media (*vide infra*). As a result, several species have been isolated, and their structural and spectroscopic properties have been well-characterized. Hence, a mononuclear species $[Co(C_4H_9O_8NP_2)(H_2O)_2]\cdot 2H_2O$ was first isolated at low pH [16], while at slightly higher pH 5.5 an assembly of species $(NH_4)_4[Co(H_2O)_6][(H_2O)_2Co(HNTA2P)$-$Co(NH_3)_2(H_2O)_3]_2[Co(NTA2P)(H_2O)_2]_2\cdot 10H_2O\cdot 1.36CH_3CH_2OH$ was isolated, providing a first insightful glimpse of the speciation in this binary system [17].

The paucity of well-defined species at high pH values and the need to investigate solid state-solution structure-properties correlations prompted us to investigate the Co(II)–NTA2P synthetic chemistry at high pH. To this end, compound $(NH_4)_3[Co(C_4H_6O_8N$-$P_2)(H_2O)_2]\cdot 4H_2O$ (**1**) was synthesized and isolated in a facile manner at pH 8. The analytical and structural properties of **1** suggest that the mononuclear species contains the diphosphonate ligand bound to Co(II) as a tetradentate ligand. Both the phosphonate and carboxylate moieties act as monodentate anchors of NTA2P to the metal ion, with the imino nitrogen being the fourth anchor due to its Lewis basic character. The two remaining coordination sites were filled with water ligands from the reaction medium. The NTA2P ligand is a quintuply deprotonated ligand, with the sites of deprotonation being both the phosphonate moieties and the carboxylate group. Varying deprotonation states linked to variable modes of phosphonate coordination had been previously observed in a number of metal organophosphonate complexes containing phosphonate ligand terminals [44]. A characteristic example is the iminodiphosphonate ligand H_4IDA2P (dubbed IDA2P) anchored onto octahedral Co(II), with a coordination mode typical of a singly deprotonated phosphonate terminal group on

either side of the central imino group. IDA2P ligand can be viewed as a derivative of the iminodiacetic acid ligand HOOC–CH_2–NH–CH_2–COOH (H_2IDA dubbed IDA), where the two terminal carboxylates are replaced by phosphonates [45,46]. Along the same lines, solution and synthetic studies with a number of aminoalkylphosphonates and IDA derivative phosphonate ligands, like N-(phosphonomethyl) glycine [47], have been carried out in the presence of metal ions [48,49]. The studies suggest that these ligands react expediently with metal ions, such as Co(II), forming soluble metal chelates. For a number of such complexes proposed to exist in solution, the thermodynamic parameters were determined and greater stability was suggested for several of the aminophosphonate versus aminocarboxylate metal species [48c].

Structural comparison of **1** with congener species in the same binary system (**3** and **4**) reveal that (a) mononuclear species exist in both low and high pH values, in line with the aqueous speciation distribution of the binary Co(II):NTA2P system and the structural characterization of the synthesized and isolated species so far, (b) the coordination geometry is octahedral at both low and high pH values of aqueous media from which the various well-characterized species are isolated. Higher pH values favor tetrahedral Co(II) coordination, (c) the bulk, steric requirements of the NTA2P ligand and its coordination properties around divalent metal ions necessitate the presence of two water molecules, saturating the octahedral coordination sphere of Co(II).

Further comparison of the properties of the pH-structural variants **1** and **3** reveal that qualitative spectroscopic and structural changes did occur in the mononuclear species, including (a) a bathochromic shift of the main absorption band (540 nm (**1**) versus 550 nm (**3**)) in the UV–Vis spectra with decreasing pH, and (b) lower frequency shifts in the observed FT-IR pattern of the antisymmetric and symmetric stretches of the carboxylate group vibrations, upon going from the low pH species **3** (1664 cm^{-1} and 1461–1408 cm^{-1}, respectively) to the high pH-structural variant species **1** (1590 cm^{-1} and 1400–1381 cm^{-1}, respectively).

4.2. The aqueous speciation of binary Co(II)–NTA$_x$P (x = 0–3) systems

A clear picture of the solution distribution of species, arising as a result of the binary interactions between Co(II) and the various NTA derivatives, was a firm step toward comprehending the chemistry involved and the potential species to be synthesized, isolated, and characterized. To this end, all potential ligands from NTA (an all-carboxylic acid containing species) to NTA3P (an all-phosphonic acid containing species) were examined. The species distributions derived from the binary speciation diagrams are in line with past reports [43] and denote the following: (a) as the number of phosphonic acid moieties increase in the tripodal NTA framework, the 1:2 CoA_2 stoichiometry is not supported for electrostatic and steric reasons. The tetradentate coordination of the first ligand molecule allows only the unfavored bidentate coordination of the second ligand (in the 1:2 species). The substitution of COO^- donors by PO_3^{2-} hinders further coordination of a second ligand molecule, due to the larger space requirements and the higher charge of the phosphonate group. Thus, 1:2 CoA_2 species are suggested to exist only in the case of the Co(II)–NTA and Co(II)–NTAP systems. (b) as the number of phosphonic acid moieties increases in the NTA framework, basicity of the ligand increases and the number of binary protonated species $CoAH_n$ increases. The deprotonation and possible subsequent coordination of the phosphonate arms occur in the pH region 3–6, however, the partial coordination of a protonated phosphonate residue can not be excluded. While the tetradentate coordination of NTA occurs very likely in solution, this type of coordination for the NTA-type phosphonate ligands seems to grow less and less favored as the number of the phosphonate moieties increases in the molecule. The increasing negative charge around the metal ion, with di-negatively charged methylenephosphonate arms instead of the uninegatively charged methylenecarboxylate arms, may hinder coordination of all donors to the same metal ion. The observed spectral parameters clearly prove this in the case of NTA3P. (c) A comparison of the Co(II) binding ability of the ligands with a metal to ligand ratio 1:1, at different pHs (see Supporting Information Fig. 6), shows that it is clear that until pH ~6 the presence of the phosphonate group decreases the stability; the stability order is NTA > ~NTAP > NTA2P > NTA3P. At pH>6 the order of the sequence reverses, with the presence of the phosphonate group increasing the stability. (d) in all cases of the NTA$_x$P ligands, the nitrogen atom remains coordinated to the metal ion regardless of the carboxylate or phosphonate moieties present in the bound ligand. To this end, nitrogen coordination brings about formation of five-membered rings, known for their contribution to the stability of the arising complexes. (e) At high pH, a change in the coordination geometry from octahedral to tetrahedral can be observed as the last deprotonation step does occur. The pK values of these processes, involving formation of the ternary hydroxo species, increase with the number of phosphonate arms and the charge of the complex.

In the case of the binary Co(II)–NTA2P aqueous system, the speciation diagram clearly indicates that in the physiological pH range and around it, the dominant species present at close to 100% amount is the $[CoA]^{3-}$ species. This species reflects an octahedral moiety with a fully deprotonated $NTA2P^{5-}$ ligand bound to Co(II). Such a species is reminiscent of the anion in compound **1**, with the remaining two coordination sites being occupied by solvent water molecules. The direct similarity between the species suggested by the aqueous speciation studies and the one actually synthesized, isolated and crystallographically characterized species, justifies the structural speciation approach and its power in comprehending metal ionic interactions with substrates bearing C,N,O-containing carboxy and phosphonate anchor groups. Furthermore, the two bound water molecules in the anion in **1**, being good leaving groups, suggest further chemical reactivity of **1** toward third targets of distinct nature (N,O-containing substrates of variable coordination mode and deprotonation state such as N,O-(hydroxy)carboxylate and mixed carboxyphosphonate derivatives). To this end, both aqueous solution and synthetic studies (a) reveal unequivocally detailed features of the arising species as a result of the binary interactions of Co(II) with NTA2P ligand, and (b) define the salient structural features formulating reactivity pathways in which the anion in **1** could seek ternary interactions leading to complex materials with new physicochemical properties.

The structural attributes of the interaction of NTA2P ligand toward Co(II), as a function of pH, reflect the multipotent coordination ability of the ligand and exemplify the diverse chemistry unfolding at both binary and ternary levels in aqueous media. It appears that this chemistry is reflected in the diverse nature of species arisen, isolated under variable reaction conditions and characterized as part of the developing equilibria in the aqueous binary Co(II):NTA2P system (species **1, 3**, and **4**). It is very likely that unknown species, currently eluding isolation in other areas of the speciation scheme of the binary system exist, thereby warranting further exploration through synthetic endeavors. The same applies to the remainder of the Co(II)–NTA*x*P binary systems, for which discrete species conforming to the suggestions of the respective speciation distributions are currently sought synthetically.

4.3. From binary to ternary metallo-organophosphonates

Metal organophosphonates have drawn considerable attention in the past years, with relevant materials probing a wide spectrum of potential practical applications and extending from catalysis to

electronics. Among metal phosphonates are those containing simple phosphate groups [50], monophosphonate groups [51], such as $H_2O_3P–CH_2–CH_2–COOH$, or diphosphonic acids [52], such as $H_2O_3P–R–PO_3H_2$, where the nature and length of R influence the dimensionality of the material [53]. The assembled structural networks are dependent upon a number of host features, including shape, size, and selectivity dependent intercalation, inter-layer distance, coordination site availability, etc. In this sense, diphosphonate group-containing pillared layered structures were reported for vanadium $[(VO)(H_2O)\{O_3PCH_2NH(C_2H_4)_2NHCH_2PO_3\}]$ [54], while three-dimensional phases were isolated with manganese, and cobalt $[M\{O_3PCH_2NH(C_2H_4)_2NHCH_2PO_3\}]\cdot H_2O$ (M = Mn(II), Co(II)) [55]. Based on the above, **1** and **3** are being probed as precursors in ternary synthetic processes involving N,O-containing (hydroxy)carboxylate or mixed carboxyphosphonate ligands, seeking new inorganic–organic hybrid materials with uniquely defined physicochemical properties.

5. Conclusions

An in-depth solution and synthetic investigation of the binary Co(II)–NTA*x*P systems in aqueous media revealed the diversity of binary Co(II) complexes arising as a function of pH and molecular stoichiometry. From an all-carboxylate (NTA) to an all-phosphonate composition (NTA3P), the NTA framework exemplifies key structural characteristics borne by the arising Co(II)–NTA*x*P ligand complexes. Key factors involving electronic, electrostatic and steric requirements dictate the nature of metal-chelate formation and composition of the aqueous distribution in each unique binary system. These features are amply reflected in the synthesized and isolated Co(II)–NTA2P pH-specific structural variant **1**. Comparison of **1** with congener pH-structural variant species in the same binary system denote the importance of the structural speciation approach as a powerful tool in (a) providing detailed information on binary Co(II)–carboxyphosphonate interactions, and (b) probing ternary Co–L–(N,O,P) interactions in processes leading to new materials with uniquely defined and differentiated properties from the nascent Co(II) ion. Henceforth, efforts to (a) pH-dependently synthesize and characterize new soluble forms of Co(II)–phosphonates in line with the discovered aqueous speciation schemes described herein, and (b) gain access to suitable Co(II)–phosphonates as precursors to new materials, are under way in our labs.

Acknowledgments

This work was supported by a "PENED" grant co-financed by the E.U.-European Social Fund (75%) and the Greek Ministry of Development-GSRT (25%), and by the Hungarian Research Fund (OTKA No. K77833).

Appendix A. Supplementary data

CCDC 787180 contains the supplementary crystallographic data for (**1**). These data can be obtained free of charge via http://www.ccdc.cam.ac.uk/conts/retrieving.html, or from the Cambridge Crystallographic Data Centre, 12 Union Road, Cambridge CB2 1EZ, UK; fax: (+44) 1223-336-033; or e-mail: deposit@ccdc.cam.ac.uk. Supplementary data associated with this article can be found, in the online version, at doi:10.1016/j.poly.2010.11.007.

References

[1] Q. Chen, J. Salta, J. Zubieta, Inorg. Chem. 32 (1993) 4485.
[2] E.T. Clarke, P.R. Rudolph, A.E. Martell, A. Clearfield, Inorg. Chim. Acta 164 (1989) 59.
[3] C. Bhardwaj, H. Hu, A. Clearfield, Inorg. Chem. 32 (1993) 4294.
[4] D.A. Burwell, K.G. Valentine, J.H. Timmermans, M.E. Thompson, J. Am. Chem. Soc. 114 (1992) 4144.
[5] G.L. Rosenthal, J. Caruso, Inorg. Chem. 31 (1992) 3104.
[6] M.B. Dines, P.C. Griffith, Inorg. Chem. 22 (1983) 567.
[7] M.B. Dines, P.M. DiGiacomo, Inorg. Chem. 20 (1981) 92.
[8] H. Byrd, J.K. Pike, D.R. Talham, J. Am. Chem. Soc. 116 (1994) 7903.
[9] D.M. Taylor, D.R. Williams, Trace Element Medicine and Chelation Therapy, Royal Society of Chemistry, Cambridge, 1995.
[10] S. Balachandran, R.A. Vishwakarma, S.M. Monaghan, A. Prelle, N.P.J. Stamford, F.J. Leeper, A.R. Battersby, J. Chem. Soc., Perkin Trans. 1 (1994) 487.
[11] A.R. Battersby, Acc. Chem. Res. 26 (1993) 15.
[12] L. Debussche, M. Couder, D. Thibaut, B. Cameron, J. Crouzet, F. Blanche, J. Bacteriol. 22 (1992) 7445.
[13] (a) S.L. Roderick, B.W. Matthews, Biochemistry 32 (1993) 3907;
(b) A. Ben-Bassat, K. Bauer, S.-Y. Chang, K. Myambo, A. Boosman, S. Chang, J. Bacteriol. 169 (1987) 751.
[14] M.S. Payne, S. Wu, R.D. Fallon, G. Tudor, B. Stieglitz, I.M. Turner, M. Nelson, J. Biochem. 36 (1997) 5447.
[15] S.J. Lippard, J.M. Berg, Principles of Bioinorganic Chemistry, U. Science Books, M. Valley, CA, 1994.
[16] A. Mateescu, C.P. Raptopoulou, A. Terzis, V. Tangoulis, A. Salifoglou, Eur. J. Inorg. Chem. (2006) 1945.
[17] A. Mateescu, C. Gabriel, R.G. Raptis, P. Baran, A. Salifoglou, Inorg. Chim. Acta 360 (2007) 638.
[18] H.M. Irving, M.G. Miles, L.D. Petit, Anal. Chim. Acta 38 (1967) 475.
[19] G. Anderegg, Anal. Chim. Acta 282 (1993) 485.
[20] L. Zékány, I. Nagypál, G. Peintler, PSEQUAD for Chemical Equilibria, Technical Software Distributions, Baltimore, MD, 1991.
[21] L. Zékány, I. Nagypál, D.J. Leggett (Eds.), Computational Methods for the Determination of Stability Constants, Plenum, NY, 1985.
[22] G.M. Sheldrick, SHELXS-97, Structure Solving Program, University of Göttingen, Germany, 1997.
[23] G.M. Sheldrick, SHELXL-97, Structure Refinement Program, University of Göttingen, Germany, 1997.
[24] H. Jankovics, M. Daskalakis, C.P. Raptopoulou, A. Terzis, V. Tangoulis, J. Giapintzakis, T. Kiss, A. Salifoglou, Inorg. Chem. 41 (2002) 3366.
[25] M. Matzapetakis, M. Dakanali, C.P. Raptopoulou, V. Tangoulis, A. Terzis, N. Moon, J. Giapintzakis, A. Salifoglou, J. Biol. Inorg. Chem. 5 (2000) 469.
[26] L. Kryger, S.E. Rasmussen, Acta Chem. Scand. 26 (1972) 2349.
[27] T. Glowiak, W. Sawka-Dobrowolska, B. Jezowska-Trzebiatowska, Inorg. Chim. Acta 45 (1980) L105.
[28] V.S. Sergienko, G.G. Aleksandrov, E.G. Afonin, Zh. Neorg. Khim. 42 (1997) 1291.
[29] J.-L. Song, J.-G. Mao, Y.-Q. Sun, H.-Y. Zeng, R.K. Kremer, A. Clearfield, J. Solid State Chem. 177 (2004) 633.
[30] V.S. Sergienko, E.G. Afonin, G.G. Aleksandrov, Zh. Neorg. Khim. 43 (1998) 1002.
[31] R.S. Drago, Physical Methods in Chemistry, W.B. Saunders Co., Philadelphia, 1977.
[32] A.B.P. Lever, Inorganic Electronic Spectroscopy, second ed., Elsevier, Amsterdam, 1984.
[33] (a) B.N. Figgis, Introduction to Ligand Fields, Interscience Publishers, New York, 1966;
(b) C.K. Jorgensen, Adv. Chem. Phys. 5 (1963) 33;
(c) C.J. Ballhausen, Introduction to Ligand Field Theory, McGraw-Hill Book Co., New York, 1962.
[34] (a) C. Djordjevic, M. Lee, E. Sinn, Inorg. Chem. 28 (1989) 719;
(b) G.B. Deacon, R. Philips, Coord. Chem. Rev. 33 (1980) 227.
[35] (a) D.E.C. Corbridge, J. Appl. Chem. 6 (1956) 456;
(b) R.C. Gore, Discuss. Faraday Soc. 9 (1950) 138;
(c) J.V. Bell, J. Heisler, H. Tannenbaum, J. Goldenson, J. Am. Chem. Soc. 76 (1954) 5185;
(d) L.C. Thomas, R.A. Chittenden, Spectrochim. Acta 20 (1964) 467.
[36] (a) R.A. McIvor, C.E. Hubley, Can. J. Chem. 37 (1959) 869;
(b) L.C. Thomas, R.A. Chittenden, Chem. Ind. (London) (1961) 1913.
[37] (a) D.S. Sagatys, C. Dahlgren, G. Smith, R.C. Bott, A.C. Willis, Aust. J. Chem. 53 (2000) 77;
(b) S. Shoval, S. Yariv, Agrochimica 25 (1981) 377;
(c) V. Subramanian, P.E. Hoggard, J. Agric. Food Chem. 36 (1988) 1326.
[38] R. Boca, Coord. Chem. Rev. 248 (2004) 757.
[39] M. Menelaou, A. Konstantopai, C. Mateescu, H. Zhao, C. Drouza, N. Lalioti, A. Salifoglou, Inorg. Chem. 48 (2009) 8092.
[40] P. Buglyó, T. Kiss, M. Dyba, M. Jezowska-Bojczuk, H. Kozlowski, S. Bouhsina, Polyhedron 16 (1997) 3447.
[41] D. Sanna, I. Bódi, S. Bouhsina, G. Micera, T. Kiss, J. Chem. Soc., Dalton Trans. (1999) 3275.
[42] M. Kilyen, A. Lakatos, R. Latajka, I. Labadi, A. Salifoglou, C.P. Raptopoulou, H. Kozlowski, T. Kiss, Dalton Trans. (2002) 3578.
[43] K. Sawada, W. Duan, M. Ono, K. Satoh, J. Chem. Soc., Dalton Trans. (2000) 919.
[44] (a) V.S. Sergienko, G.G. Aleksandrov, E.G. Afonin, Kristallografiya 45 (2000) 262;
(b) P.H. Smith, K.N. Raymond, Inorg. Chem. 27 (1988) 1056;
(c) T. Glowiak, W. Sawka-Dobrowolska, B. Jezowska-Trzebiatowska, A. Antonow, J. Cryst. Mol. Struct. 10 (1980) 1;
(d) P. Fenot, J. Darriet, C. Garrigou-Lagrange, J. Mol. Struct. 43 (1978) 49.

[45] (a) S.P. Petrosyants, M.A. Malyarik, A.B. Ilyukhin, Zh. Neorg. Khim. 40 (1995) 769;
(b) B.B. Smith, D.T. Sawyer, Inorg. Chem. 7 (1968) 922.
[46] (a) D. Mootz, H. Wunderlich, Acta Crystallogr., Sect. B 36 (1980) 445;
(b) N.J. Mammano, D.H. Templeton, A. Zalkin, Acta Crystallogr., Sect. B 33 (1977) 1251;
(c) A.B. Corradi, C.G. Palmieri, M. Nardelli, M.A. Pellinghelli, M.E.V. Tani, J. Chem. Soc., Dalton Trans. (1973) 655.
[47] (a) R.J. Motekaitis, A.E. Martell, J. Coord. Chem. 14 (1985) 139;
(b) H.E.L. Madsen, H.H. Christensen, C. Gottlieb-Petersen, Acta Chem. Scand. A 32 (1978) 79.
[48] (a) M. Wozniak, G. Nowogrocki, Talanta 26 (1979) 1135;
(b) M. Wozniak, G. Nowogrocki, Talanta 26 (1979) 381;
(c) T. Kiss, G. Balla, G. Nagy, H. Kozlowski, J. Kowalik, Inorg. Chim. Acta 138 (1987) 25;
(d) B. Radomska, E. Matczak-Jon, W. Woiciechowski, Inorg. Chim. Acta 124 (1986) 83;
(e) T.I. Ignat'eva, A.N. Bovin, A.V. Yarkov, A.N. Chekhlov, E.N. Tsvetkov, O.A. Raevskii, Koord. Khim. 15 (1989) 1179.
[49] (a) T. Appleton, J.R. Hall, I.J. McMahon, Inorg. Chem. 25 (1986) 726;
(b) R.J. Motekaitis, I. Murase, A.E. Martell, Inorg. Chem. 15 (1976) 2303.
[50] A. Choudhury, S. Natarajan, Solid State Sci. 2 (2000) 365.
[51] (a) G. Cao, V.M. Lynch, J.S. Swinnea, T.E. Mallouk, Inorg. Chem. 29 (1990) 2112;
(b) G.B. Hix, V.J. Carter, D.S. Wragg, R.E. Morris, P.A. Wright, J. Mater. Chem. 9 (1999) 179.
[52] (a) S. Drumel, P. Janvier, P. Barboux, M. Bujoli-Doeuff, B. Bujoli, Inorg. Chem. 34 (1995) 148;
(b) S. Drumel, P. Janvier, P. Barboux, M. Bujoli-Doeuff, B. Bujoli, New J. Chem. 19 (1995) 239.
[53] V. Soghomonian, Q. Chen, R.C. Haushalter, J. Zubieta, Angew. Chem., Int. Ed. Engl. 34 (1995) 223.
[54] V. Soghomonian, R. Diaz, R.C. Haushalter, C.J. O'Connor, J. Zubieta, Inorg. Chem. 34 (1995) 4460.
[55] R. LaDuca, D. Rose, J.R.D. DeBord, R.C. Haushalter, C.J. O'Connor, J. Zubieta, J. Solid State Chem. 123 (1996) 408.